A Context-Aware Cognitive SIMO DL Transceiver for LTE HetNet Power Efficiency and Throughput Enhancement

Imen Mrissa, Faouzi Bellili, Sofiène Affes, and Alex Stéphenne
INRS-EMT, 800 De La Gauchetiere Ouest, Suite 6900, Montreal (Quebec), H5A 1K6, Canada.
Emails: {mrissa, bellili, affes}@emt.inrs.ca and stephenne@ieee.org

***Abstract*—In this paper, we propose a new single-input multiple-output (SIMO) context-aware cognitive transceiver (CTR) that is able to switch to the best performing modem in terms of link-level throughput and allows to decrease macro transmission power without loosing performances. On the top of conventional adaptive modulation and coding (AMC), we allow the context-aware CTR to make best selection among three different pilot-utilization modes: conventional data-aided (DA) or pilot-assisted, non-DA (NDA) or blind, and NDA with pilot which is a newly proposed hybrid version between the DA and NDA modes. We also enable the CTR to make best selection between two different channel identification schemes: conventional least-squares (LS) and newly developed maximum-likelihood (ML) estimators. Depending on whether pilot symbols can be properly exploited or not at the receiver, we further enable the CTR to make best selection among two data detection modes: coherent or differential. It will be seen that the new cognitive transceiver allows to 1) decrease macro transmission power to the half (typically from 40 to 20 Watts), and 2) achieve an average throughput gain as high as 140% and a 5^{th} percentile throughput gain reaching 230% for pico-cells in case of low UE clustering distributions.**

I. Introduction

The rapidly increasing demand for mobile radio services causes a bottleneck challenge for all wireless communication systems. Deploying Heterogeneous Networks (HetNets) has been envisaged in order to resolve this issue that is further exacerbated with the limited frequency resources. The basic concept of a HetNet technology consists in depolying additional low-power nodes in a macro-cell layout. Small cells provide additional radio resources and hence guarantee a cost-effective system capacity and throughput improvement. However, as the transmission power of pico-cells is 40 times smaller than that of macro-cells, the former are subject to very high levels interference. This interference issue entails the following two major problems: i) limited coverage area for small-cells. ii) low throughput performances as user equipments (UEs) served by small-cells experience low signal-to-interference-plus-noise ratios (SINR). In the literature, many solutions are proposed to mitigate interference problems and enhance the performance of HetNet systems [1]- [5]. Decreasing macro transmission power which can resolve both of the aforementioned issues, at the cost, however, of degrading the overall macro-cell performance. In this paper, we design a new cognitive transceiver (CTR) that is able to handle those conflicting small-/macro-cells' power requirements. It will be seen that the proposed CTR provides indeed considerable throughput gains for both pico and macro-cells by decreasing the macro transmission power. More specifically, the new CTR saves half of the macro transmit power while ensuring an overall system throughput gain of about 60%.

The remainder of this paper is structured as follows. In Section II, we introduce the context-aware CTR modes along with the different associated channel estimation schemes. In Section III, exhaustive computer simulations are presented and discussed in order to assess and illustrate the tremendous performance gains offered by the proposed CTR. Finally, concluding remarks are drawn out in Section IV.

Work supported by the CREATE PERSWADE <www.create-perswade.ca> and the Discovery Grants Programs of NSERC and a Discovery Accelerator Supplement (DAS) Award from NSERC.

II. Context-aware cognitive transceiver modes

A. DA or pilot-assisted mode

Pilot symbols are reference (i.e., known) symbols inserted according to a predefined mapping to be used by the receiver for channel estimation and synchronization purposes.

1) LS channel estimator: This conventional estimator uses pilot symbols to estimate the channel by minimizing the squared difference between the received signal and the known pilot symbols. Let $y_{i,\text{DA}}(t)$ denote the received signal (at the output of the DFT block) on pilot sub-carrier i among N_{pilot} pilot sub-carriers at the OFDM (pilot) symbol index t. For convenience, we will henceforth omit the time index t. The transmitted pilot symbol $x_{i,\text{DA}}$ is related to $y_{i,\text{DA}}$ as follows:

$$y_{i,\text{DA}} = h_i x_{i,\text{DA}} + w_i \qquad i = 0, 1, ..., N_{pilot} - 1 \tag{1}$$

where h_i is the complex channel (frequency response) coefficient and w_i is a zero-mean Gaussian noise. The matrix notation of (1) is given by:

$$\mathbf{y}_{\text{DA}} = \mathbf{X}_{\text{DA}}\mathbf{h} + \mathbf{w} \tag{2}$$

where $\mathbf{X}_{\text{DA}} = \text{diag}\left\{x_{0,\text{DA}}, x_{1,\text{DA}}, \ldots, x_{N_{pilot}-1,\text{DA}}\right\}$, $\mathbf{h} = [h_0, h_1, ..., h_{N_{pilot}-1}]^T$, and $\mathbf{w} = [w_0, w_1, ..., w_{N_{pilot}-1}]^T$ is the i.i.d complex zero-mean Gaussian noise vector. The LS algorithm minimizes $(\mathbf{y}_{\text{DA}} - \mathbf{X}_{\text{DA}}\mathbf{h})^{\dagger}(\mathbf{y}_{\text{DA}} - \mathbf{X}_{\text{DA}}\mathbf{h})$ ($\dagger$ denotes matrix Hermitian transpose) to estimate the channel frequency response at pilot positions thereby leading to [6]:

$$\widehat{\mathbf{h}}_{\text{LS}} = \mathbf{X}_{\text{DA}}^{-1}\mathbf{y}_{\text{DA}}, \tag{3}$$

where $\mathbf{A}^{-1}$ denotes matrix inverse. The estimates for the channel coefficients at non-pilot subcarriers can then be easily obtained by interpolation [9]. However, when the channel is fast fading (i.e., high user velocity), the underlyingpilot symbols spacing may not be sufficient for proper tracking of the channel time variations. Note here that decreasing pilot spacing increases pilot overhead thereby limiting the throughput which is not desirable for any communication system.

2) ML estimator: Here, we consider the ML channel estimator recently developed in [7]. Over consecutive OFDM symbols, the DA ML estimator captures the channel's time variations via a polynomial-in-time expansion of order $(J-1)$. In fact, the channel over each $\{r^{th}\}_{r=1}^{N_r}$ antenna branch and the i^{th} subcarrier, is modeled as follows [8]:

$$h_{i,r}(t_n) = \sum_{j=0}^{J-1} c_{i,r}^{(j)} t_n^j + REM_J^{(i,r)}(t_n). \tag{4}$$

Here, $t_n = nT_s$ with T_s being the OFDM symbol period. The polynomial order $J-1$ is a Doppler-dependent parameter optimized in [7]. Moreover, $c_{i,r}^{(j)}$ is the j^{th} coefficient of the underlying channel polynomial approximation over the i^{th} sub-carrier and

978-1-4673-6555-0/15/$31.00 ©2015 IEEE

the r^{th} antenna element. As will be explained shortly, the term $REM_J^{(i,r)}(t_n)$ which refers to the remainder of the Taylor series expansion can be driven to zero by dividing the entire observation window into multiple local approximation windows of sufficiently small sizes. Therefore, the channel can be locally approximates as follows [7]:

$$h_{i,r}(t_n) = \sum_{j=0}^{J-1} c_{i,r}^{(j)} t_n^j. \quad (5)$$

Channel estimation is performed independently over each pilot sub-carrier. For the sake of simplicity, we also omit the sub-carrier index in the remainder of this paper since the very same estimation procedure applies for all sub-carriers.

To use a small model order, $J-1$, in (4) and avoid costly inversions of large-size matrices, the new DA ML estimator partitions the whole observation window into K local approximation windows of the same size. Then, it maximizes the probability density function (pdf) of the locally-observed vectors, $\mathbf{y}_{\text{DA}}^{(k)}$, parametrized by $\mathbf{c}_k$:

$$p(\mathbf{y}_{\text{DA}}^{(k)};\mathbf{c}_k|\mathbf{B}_k) = \frac{1}{(2\pi\sigma^2)^{N_{\text{DA}}N_r}} \exp\left\{-\frac{1}{2\sigma^2}\left[\mathbf{y}_{\text{DA}}^{(k)}-\mathbf{B}_k\mathbf{c}_k\right]^H\left[\mathbf{y}_{\text{DA}}^{(k)}-\mathbf{B}_k\mathbf{c}_k\right]\right\}, \quad (6)$$

where σ^2 is the noise variance and $\mathbf{c}_k$ is a vector that contains the unknown polynomial approximation coefficients, for all the antenna branches, over the k^{th} approximation window, defined as $\mathbf{c}_k = [\mathbf{c}_{k,1}^T, \mathbf{c}_{k,2}^T, ..., \mathbf{c}_{k,N_r}^T]^T$. Here $\mathbf{c}_{k,r} = [c_{k,r}^{(0)}, c_{k,r}^{(1)}, ..., c_{k,r}^{(J-1)}]^T$ with $c_{k,r}^{(j)}$ being the j^{th} coefficient of the polynomial approximation over the i^{th} sub-carrier, the k^{th} approximation window, and the r^{th} antenna branch. Moreover, in (6), $\mathbf{y}_{\text{DA}}^{(k)} = [\mathbf{y}_{1,\text{DA}}^{(k)}\, \mathbf{y}_{2,\text{DA}}^{(k)} \dots \mathbf{y}_{N_r,\text{DA}}^{(k)}]^T$ with $\mathbf{y}_{r,\text{DA}}^{(k)}$ being the received pilot samples over the antenna element r within the k^{th} approximation window, i.e., $\mathbf{y}_{r,\text{DA}}^{(k)} = [y_r^{(k)}(t_1)\, y_r^{(k)}(t_2) \dots y_r^{(k)}(t_{P_{\text{DA}}})]$. Here P_{DA} is the number of pilot symbols in each approximation window which is covering N_{DA} pilot and non-pilot received samples. The approximation window size N_{DA} is another Doppler-dependent design parameter optimized in [7]. Moreover $\mathbf{B}_k$ is a $P_{\text{DA}}N_r \times JN_r$ block-diagonal matrix defined as $\mathbf{B}_k = \text{blkdiag}\{\mathbf{A}_k\mathbf{T}, \mathbf{A}_k\mathbf{T}, ..., \mathbf{A}_k\mathbf{T}\}$. Here, $\mathbf{A}_k$ is the $P_{\text{DA}} \times P_{\text{DA}}$ diagonal matrix of the transmitted pilot symbols within the k^{th} observation window, i.e., $\mathbf{A}_k = \text{diag}\{a_k(t_1), a_k(t_2), ..., a_k(t_{P_{\text{DA}}})\}$, and $\mathbf{T}$ is a Vandermonde matrix given by:

$$\mathbf{T} = \begin{pmatrix} 1 & t_1 & ... & t_1^{J-1} \\ 1 & t_2 & ... & t_2^{J-1} \\ \vdots & \vdots & \ddots & \vdots \\ 1 & t_{P_{DA}} & ... & t_{P_{DA}}^{J-1} \end{pmatrix}. \quad (7)$$

The estimate of the channel coefficients over all the receiving antenna branches are obtained by setting the partial derivative of (6) [or its natural logarithm] to zero leading to:

$$\widehat{\mathbf{c}}_{k,\text{DA}} = (\mathbf{B}_k^\dagger\mathbf{B}_k)^{-1}\mathbf{B}_k^\dagger\mathbf{y}_{\text{DA}}^{(k)}, \quad (8)$$

from which the DA ML estimates for the channel coefficients, at both pilot and non-pilot positions, are obtained by injecting the estimates of the polynomial coefficients established in (8) back into (4).

B. NDA with pilot or hybrid mode

Ensuring reliable communications is the purpose of all wireless communication systems. However, receiver mobility and surrounding scatterers' motion make accurate estimation of highly time-varying channels a truly challenging task. In fact, relying only on pilot symbols that are often inserted far apart, in the time-frequency grid, do not enable accurate tracking of fast-varying channels. Information carried in data symbols is also exploited hereafter in a hybrid channel identification scheme in order to enhance the system performance.

1) NDA w. pilot RLS estimator: At OFDM symbol $t+1$, we use the preceding transmitted signals as a training sequence of t symbols. In fact, the channel estimate, $\widehat{\mathbf{H}}_{t+1}$, at OFDM symbol $t+1$ is obtained using the weighted LS method as follows [10]:

$$\widehat{\mathbf{H}}_{t+1} = \underset{\widehat{\mathbf{H}}}{\text{argmin}} \sum_{w=1}^{t} \beta_w \|\mathbf{y}_w - \widehat{\mathbf{H}}\mathbf{Q}_w x_w\|^2, \quad (9)$$

where the channel variation $\mathcal{H}$ is approximated to the D^{th} order Taylor series expansion according to the OFDM symbol instance m, i.e.: $\mathcal{H}_w \simeq \sum_{d=0}^{D} w^d \mathcal{H}^{<d>} = \mathbf{H}\mathbf{Q}_w$ with $\mathbf{Q}_w \triangleq [w^0\mathbf{I}_{N_r}, w^1\mathbf{I}_{N_r}, ..., w^D\mathbf{I}_{N_r}]^T \in \mathbb{R}^{N_r(D+1)\times N_r}$. In (9) $\beta_w \in \mathbb{R}$ stands for a weighting coefficient given by $\beta_w = \lambda^{t-w}$ where $\lambda \in \mathbb{R}$ is the so-called forgetting factor. The exponential-weighted RLS algorithm is implemented as follows [10]:

$$\begin{aligned} \boldsymbol{\zeta}_t &= \boldsymbol{\Phi}_{t-1}^{-1}\mathbf{Q}_t x_t \in \mathbb{C}^{N_r(D+1)\times 1}, \\ \alpha_t &= \frac{1}{\lambda + \boldsymbol{\zeta}_t^\dagger \mathbf{Q}_t x_t} \in \mathbb{R}, \\ \boldsymbol{\Phi}_t^{-1} &= \lambda^{-1}\boldsymbol{\Phi}_{t-1}^{-1} - \lambda^{-1}\alpha_t\boldsymbol{\zeta}_t\boldsymbol{\zeta}_t^\dagger \in \mathbb{C}^{N_r(D+1)\times N_r(D+1)}, \\ e_t &= y_t - \widehat{\mathbf{H}}x_t \in \mathbb{C} \\ \widehat{\mathbf{H}}_{t+1} &= \widehat{\mathbf{H}}_t + \alpha_t e_t \zeta_t^\dagger \in \mathbb{C}^{1\times N_r(D+1)}. \end{aligned}$$

As initialization, $\widehat{\mathbf{H}}_1$ is considered to be identically zero and $\boldsymbol{\Phi}_0^{-1}$ is set to $\varrho\mathbf{I}_{N_r(D+1)}$ where $\varrho \gg 1$ is some constant with sufficiently large value. Moreover, x_1 is assumed to be a pilot symbol. The channel estimate $\widehat{\mathbf{H}}_{t+1}$ is then used to detect the $(t+1)^{th}$ symbol x_{t+1}.

2) NDA w. pilot ML estimator: We consider the expectation maximization (EM)-based ML estimator developed in [7]. The new estimator uses pilot and data symbols jointly in order to track the channel variations. In a first step and for a given sub-carrier, the NDA with pilot estimator relies on pilot symbols to estimate the channel coefficients at pilot OFDM symbols as described previously in Section II-A2. In a second step, the NDA with pilot estimator applies the EM algorithm over all the received samples (i.e., pilots and non-pilots) in order to jointly estimate the channel coefficients and detect the unknown data symbols. The iterative EM algorithm runs in two main steps and uses as initialization $\widehat{\mathbf{c}}_{k,\text{DA}}$ obtained in (8) from pilot positions only.

• Expectation step (E-Step):

During the E-Step, the pdf defined in (6) takes into account all the possible transmitted symbols $\{a_m\}_{m=1}^M$ where M is the modulation order. In fact, at each EM iteration q , and within each k^{th} approximation window of size N_{NDA} symbols, the objective function is updated as follows:

$$\begin{aligned} Q(\mathbf{c}_k \mid \widehat{\mathbf{c}}_k^{(q-1)}) &= -N_{\text{NDA}}N_r \ln(2\pi\sigma^2) \\ &- \frac{1}{2\sigma^2}\sum_{r=1}^{N_r}\left(M_{2,k}^{(r)} + \sum_{n=1}^{N_{\text{NDA}}} \alpha_{n,k}^{(q-1)} |\mathbf{c}_{r,k}^T\mathbf{t}(n)|^2 - 2\beta_{r,n,k}^{(q-1)}(\mathbf{c}_{r,k})\right), \quad (10) \end{aligned}$$

where $M_{2,k}^{(r)} = E\{|y_{r,k}(n)|^2\}$ is the second-order moment of the received samples over the r^{th} receiving antenna branch, $\mathbf{t}(n) = [1, t_n, t_n^2, ..., t_n^{J-1}]^T$ and:

$$\alpha_{n,k}^{(q-1)} = \sum_{m=1}^{M} P_{m,n,k}^{(q-1)} |a_m|^2, \quad (11)$$

$$\beta_{r,n,k}^{(q-1)}(\mathbf{c}_{r,k}) = \sum_{m=1}^{M} P_{m,n,k}^{(q-1)} \Re\{y_{r,k}^{*}(n) a_m \mathbf{t}^T(n) \mathbf{c}_{i,k}\}. \quad (12)$$

Here, $P_{m,n,k}^{(q-1)} = P(a_m \mid \mathbf{y}_k(n); \widehat{\mathbf{c}}^{(q-1)})$ is the *a posteriori* probability of a_m at iteration $(q-1)$ that is computed using the Bayes' formula as follows:

$$P_{m,n,k}^{(q-1)} = \frac{P(a_m) P\left(\mathbf{y}_k(n) | a_m; \widehat{\mathbf{c}}_k^{(q-1)}\right)}{P\left(\mathbf{y}_k(n); \widehat{\mathbf{c}}_k^{(q-1)}\right)}. \quad (13)$$

Since the transmitted symbols are assumed to be equally likely, we have $P(a_m) = \frac{1}{M}$ and therefore:

$$P\left(\mathbf{y}_k(n); \widehat{\mathbf{c}}_k^{(q-1)}\right) = \frac{1}{M} \sum_{m=1}^{M} P\left(\mathbf{y}_k(n) | a_m; \widehat{\mathbf{c}}_k^{(q-1)}\right). \quad (14)$$

• Maximization step (M-Step):

During the M-Step, the objective function obtained in (10) is maximized with respect to $\mathbf{c}_k$:

$$\widehat{\mathbf{c}}_k^{(q)} = \underset{\mathbf{c}_k}{\operatorname{argmax}}\, Q(\mathbf{c}_k | \widehat{\mathbf{c}}_k^{(q-1)}), \quad (15)$$

yielding the following more refined estimates for the polynomial approximation coefficients:

$$\widehat{\mathbf{c}}_{r,k}^{(q)} = \left(\sum_{n=1}^{N_{\text{NDA}}} \mathbf{t}(n) \mathbf{t}^T(n) \right)^{-1} \sum_{n=1}^{N_{\text{NDA}}} \lambda_{r,n,k}^{(q-1)} \mathbf{t}(n). \quad (16)$$

In (16), $\lambda_{r,n,k}^{(q-1)}$ is given by:

$$\lambda_{r,n,k}^{(q-1)} = \left[\widehat{a}_k^{(q-1)}(t_n) \right]^{*} y_{r,k}(t_n), \quad (17)$$

in which

$$\widehat{a}_k^{(q-1)}(t_n) = \sum_{m=1}^{M} P_{m,n,k}^{(q-1)} a_m, \quad (18)$$

is the soft symbol estimate at iteration $q-1$ and $\mathbf{t}(\text{n}) = [1, t_n, t_n^2, ..., t_n^{J-1}]^T$.

C. NDA or blind mode

For blind or NDA channel estimation, no pilot symbols are exploited by the receiver. Channel estimation is performed based on the information carried by all the symbols which are assumed to be *a priori* unknown. Phase ambiguity is resolved by differential modulation. The blind RLS channel estimator algorithm is already the one described in Section II-B1. However, an arbitrary guess of the first transmitted symbol is used to initialize the underlying recursive algorithm. The blind channel estimation algorithm is also the one described in Section II-B2. The only difference, however, is that initialization is arbitrary and random.

D. Data detection modes

On the top of selecting the appropriate channel estimator and pilot-use couples among DA ML, NDA w. pilot ML, NDA ML, DA LS, NDA w. pilot RLS and NDA RLS, the new context-aware CTR selects one of the following data detection modes:
• Coherent if pilot symbols are used.
• Non coherent or differential if no pilot symbols are used.
We also implement a "fully differential" transceiver version for which no channel estimation is required and data detection is based on differential modulation-demodulation only. We use the soft-decision-aided DAPSK detection algorithm developed in [11] and [12].

III. Simulation setup and results

A (1×2) antenna configuration (1 transmit antenna at the eNodeB and 2 receive antennas at the mobile) is adopted as a SIMO configuration example for discussion in this section. Exhaustive computer simulations will be conducted in order to assess the performance of the newly proposed CTR at both the link- and system-levels.

A. Link-level simulations

In this subsection, link-level simulations assuming only one base station and a single mobile user are used to draw decision rules regarding:

1) The best channel identification mode [among DA, NDA w. pilot (i.e., hybrid), and completely NDA] that yields the highest link-level throughput.
2) The best detection scheme between coherent and differential depending on whether pilot symbols can be properly exploited or not at the receiver, respectively.
3) The best modulation/coding channel quality indicator (CQI) couple among the conventional coherent (CQI-C) and the newly-designed differential (CQI-D) ones.

The decision rules are drawn out against the operating conditions in terms of the signal-to-noise ratio (SNR), channel model type, mobile speed, and CQI value. Most significant LTE DL link-level parameters are summarized in Tab. I.

TABLE I. Link-level simulations parameters.

Number of User Equipments	1
Channel bandwidth (MHz)	15
Carrrier frequency (GHz)	2.1
Frame duration (ms)	10
Subframe duration (ms)	1
Number of resource blocks	75
Number of subcarriers/RB	12
OFDM symbols per subframe	7
Transmit mode	SIMO
Channel types	PedA, VehA, and VehB
Channel coding	Convolutional turbo encoder

We consider a Pedestrian A (PedA) flat-fading channel model for users with mobile speed of 2 km/h and Vehicular A (VehA) and B (VehB) frequency-selective channels for users with mobile speeds of 30 km/h and 100 km/h, respectively. Their power delay profiles (PDPs) are given in [16]. In order to account for adaptive modulation and coding (AMC), a CQI value indicates to the eNodeB the modulation order and the channel coding rate adopted in each subframe. The CQI value ranges between 1 and 15 defining, respectively, six, three, and six possible coding rates for QPSK/DQPSK, 16QAM/D16Star-QAM, and 64QAM/D64Star-QAM modulations [15]. Note that CQI-C and CQI-D stand for coherent and differential detection modulations, respectively. In our simulations, the CQI values as well as the SNR are assumed to be perfectly known at the receiver side. Assessment of CQI feedback and delay errors are beyond the scope of this contribution.
Our proposed CTR switches between the fully differential mode and the different LS and ML channel estimation schemes: namely DA LS, NDA w. pilot LS, NDA LS, DA ML, NDA w. pilot ML, and NDA ML. We present in Fig. 1 the associated link-level throughput gains over the DA LS considered as a global reference. We present the gains for each triplet of (channel type, mobile speed, SNR/CQI value). As seen from Fig. 1, the gains offered by the proposed CTR over the conventional DA LS transceiver (with no cognition) can reach 700% in the low-SNR region for VehB channel and mobile speed of 100 kmph.

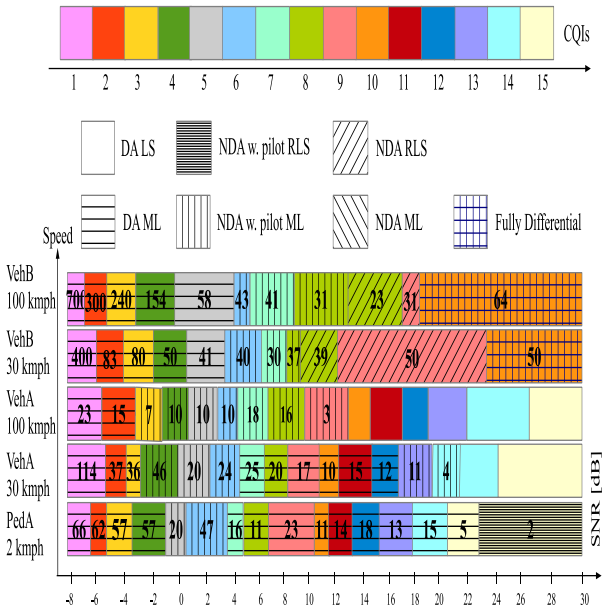

Fig. 1. Decision rules of the proposed CTR and the associated throughput gain percentages against the conventional DA LS receiver (with coherent detection) versus SNR, for different channel types and mobile speeds.

B. System-level simulations

The link-level-based decision rules, identified in the previous subsection, are then assigned to a HetNet LTE DL system-level simulator in order to assess the performance of the new cognitive transceiver under more realistic conditions that take into account the interference effects of all network elements. Macro-cell transmit power is 40 times higher than that of pico-cells making the latter prone to very high interference levels. Our goal is to reduce the transmit power of macro-cells without scarifying, however, their performance while enhancing at the same time pico-cells' performance. To that end, we simulate a DL LTE-HetNet consisting of 7 hexagonal macro-cells with pico-cells being dropped randomly in each macro area. We also consider low and high UE clustering distributions. For low clustering, 4 UEs are dropped in each hotspot (pico-cell area) and the remaining are dropped uniformly in the entire cell-site area. For high clustering, however, $\frac{2}{3}$ of the UEs are dropped in the total hotspots and the remaining are dropped uniformly in the whole cell-site area. Each UE selects its serving cell (i.e., macro or pico) by comparing the corresponding received signal strength. Since pico-cells transmit much weaker power levels than the hosting macro-cell, UEs tend to select the latter as the serving cell in most of cases (i.e., very rare UEs offloading to pico-cells). Reducing macro-cell transmission power is an immediate solution that allows one to enhance the coverage range of pico-cells at the cost, though, of reducing macro-cells' performance. In this contribution, we succeed, however, in reducing macro-cell transmit power while achieving macro performances enhancements owing to the CTR introduced in Section II. Typically, we decrease macro transmit power from 40 to 30 and 20 Watts. We simulate a co-channel pico-cell deployment for which macro and pico-cells share the same radio resources. An exhaustive list of the system-level parameters we used during our simulations is provided in Tab. II. We also assume that 50% of the users move at a speed of 2 km/h and experience PedA channel type. The remaining 30% and 20% of the users are assumed to move at medium and high speeds of 30 and 100 km/h, respectively. Medium and high-speed users experience VehA channel type and we simulate $\{1, 2, 4\}$ pico-cells per macro area as defined in [14]. Fig. 3 shows that reducing the macro-cell transmit power increases the number of UEs assigned to pico-cells for low and high UE clustering distributions. Fig. 2 shows the throughput CDFs for the whole cell-site, the macro-cells and

TABLE II. SYSTEM-LEVEL SIMULATION PARAMETERS.

Macrocell parameters	
Inter-site distance	500 meters
Minimum UE to macro-BS distance	35 meters
Path loss model	TS 36.942, subclause 4.5.2
Antenna pattern	3-dimensional TS 36.942
TX antennas	1
Shadowing	Log-normal with 10 dB standard deviation
LTE BS antenna gain after cable loss	17 dBi
Maximum macro-BS TX power	46 dBm (conventional), 44.77 dBm and 43 dBm
Scheduling algorithm	Proportional Fair
Resource Block width	180 kHz, total 12 RBs per subframe
Pico-cell parameters	
Minimum distance between pico pNodeBs	40 meters
Minimum distance between new node and regular nodes	75 meters
Path loss model	TS 36.942, subclause 4.5.2
Antenna pattern	Omnidirectional
Antenna gain	5 dBi
Maximum pico-DS TX power	30 dBm
UE parameters	
UE Rx antennas	2
Number of UEs per cell-site	60

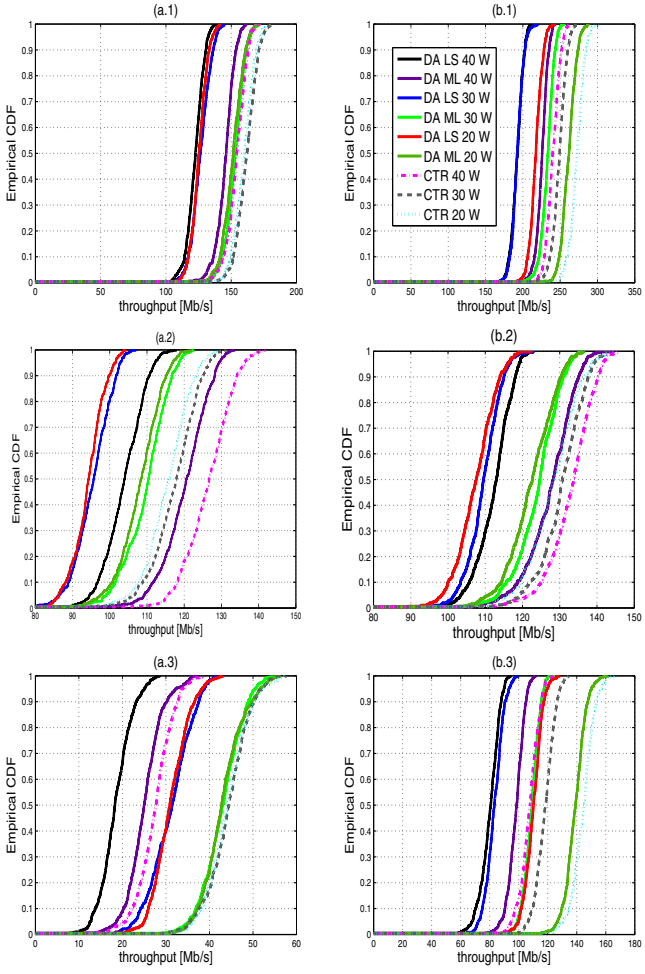

Fig. 2. System-level throughput empirical CDF for a) low clustering with 2 pico-cells per cell-site, b) high clustering with 4 pico-cells per cell-site; 1) per cell-site, 2) per macro-cell, and 3) per pico-cell.

pico-cells in case of low and high UE clustering distribution[1]. It is seen that, unlike macro-cell, pico-cells experience considerable performance enhancements by reducing macro transmit power; under the three transceiver architectures (i.e., DA LS, DA ML, and CTR). Throughput improvements are, however, more prominent with CTR. As far as the whole cell-site performance is concerned, Fig. 2 also shows that CTR offers the best throughput CDFs

[1]Note here that due to space limitations we only show results for 2 and 4 dropped pico-cells in case of low and high clustering UEs distribution respectively.

with only 20 instead of 40 Watts of macro transmitted power. Finally, Fig. 4 depicts the relative gains offered by the proposed CTR (with a macro Tx power of 20 Watts) over the conventional DA LS with a macro Tx power of 40 Watts. There, it is seen that CTR offers a gain as high as 230% and 140% for average and cell-edge throughputs, respectively, for pico-cells in case of low UE clustering distributions. On the other hand, the whole cell-site benefits from an average and 5^{th} percentile throughput gain that reaches 60%. Macro-cells, as well, despite having their corresponding transmit power reduced to 20 Watts show a considerable throughput gain of about 30% with our CTR as compared to the conventional DA LS transceiver with Tx power of 40 Watts.

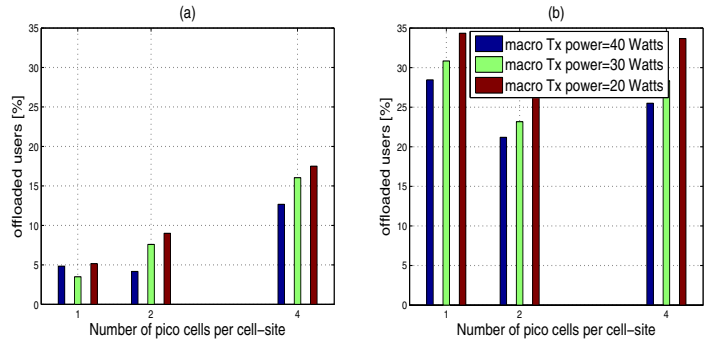

Fig. 3. Percentage of offloaded users to pico-cells for (a) low clustering and (b) high clustering.

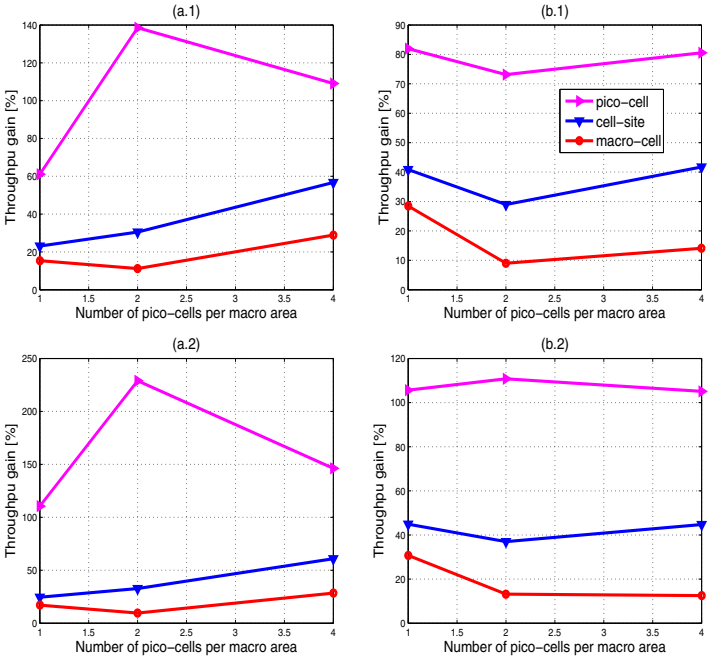

Fig. 4. System-level throughput gains for (a) low clustering and (b) high clustering; 1) average, and 2) cell-edge (or 5^{th} percentile).

IV. Conclusion

In this paper, we developed a new SIMO context-aware cognitive transceiver (CTR) that is able to switch to the best performing modem in terms of link-level throughput. On the top of conventional adaptive modulation and coding (AMC), we allowed the proposed CTR to make best selection among three different pilot-utilization modes: conventional DA (or pilot-assisted), completely NDA (or blind), and NDA with pilot which is a newly proposed hybrid version between the DA and NDA modes. We also enabled the underlying CTR to make best selection between two different channel identification schemes: conventional least-squares (LS) and newly developed maximum-likelihood (ML) estimators. Depending on whether pilot symbols can be properly exploited or not (at the receiver), we further enabled the CTR to make best selection among two data detection modes: coherent or differential. Owing to extensive and exhaustive simulations on the downlink (DL) of a long-term evolution (LTE) heterogeneous networks (HetNets), we were able to draw out the optimal decision rules of the new CTR that identify the best combination triplet of (pilot-use, channel-identification, and data-detection mode). The identified decision rules correspond to the best link-level throughput at any operating condition in terms of channel type, mobile speed, SNR, and CQI. The proposed CTR allows the deployment of environment-friendly base stations, within the framework of LTE HetNets, as it entails huge power savings by reducing macro-cell transmit powers to the half (from 40 to 20 Watts). Besides power efficiency enhancement, CTR also offers relative cell-site throughput gain of about 60% over the conventional non-cognitive DA LS transceiver.

References

[1] B. Soret and K. I. Pedersen, "Macro transmission power reduction for HetNet co-channel deployments," in *Proc of IEEE Global Communications Conference (GLOBECOM)*, Anaheim, CA, Dec. 2012, pp. 4126 - 4130.

[2] Madan, R. J. Borran, A. Sampath, N. Bhushan, A. Khandekar, and J. Tingfang, "Cell association and interference coordination in heterogeneous LTE-A cellular networks," *IEEE Journal on Selected Areas in Communications*, vol. 28, no. 9, pp. 1479-1489, Dec. 2010.

[3] K. Okino, T. Nakayama, C. Yamazaki, H. Sato, Y. Kusano, "Pico cell range expansion with interference mitigation toward LTE-Advanced heterogeneous networks," in *Proc of IEEE International Conference on Communications Workshops (ICC)*, Kyoto, June. 2011.

[4] K. Kikuchi, H. Otsuka, "Proposal of adaptive control CRE in heterogeneous networks," in *Proc of IEEE 23rd International Symposium on Personal Indoor and Mobile Radio Communications (PIMRC)*, Sydney, NSW, Sept. 2012.

[5] S. Strzyz, K. I. Pedersen, J. Lachowski, F. Frederiksen, "Performance optimization of pico node deployment in LTE macro cells," in *IEEE Future Network and Mobile Summit (FutureNetw)*, Warsaw, June. 2011.

[6] J. J. Van de Beek, *et al*, "On channel estimation in OFDM systems," in *Proc of IEEE 45th Vehicular Technology Conference* , Chicago, IL, July. 1995, vol. 2, pp. 815-819.

[7] F. Bellili, R. Meftehi, S. Affes, and A. Stéphenne, "Maximum likelihood SNR estimation of linearly-modulated signals over time-varying flat-fading SIMO channels," *IEEE Transactions on Signal Processing,*, vol. 63, no. 2, pp. 441-456. Jan. 2015.

[8] P. Bello, "Characterization of randomly time-variant linear channels," *IEEE Transactions on Communications Systems.*, vol. 11, no. 4, pp. 360-393, Dec. 1963.

[9] S. Omar , A. Ancora, and D.T.M. Slock, "Performance analysis of general pilot-aided linear channel estimation in LTE OFDMA systems with application to simplified MMSE schemes," in *Proc of IEEE 19th International Symposium on Personal, Indoor and Mobile Radio Communications (PIMRC)* , Cannes, sept. 2008, p. 1-6.

[10] T.K. Akino, "Optimum weighted RLS channel estimation for rapid fading mimo channels," *IEEE Transactions on Wireless Communications*, vol. 7, no. 11, pp. 4248-4260, Nov. 2008.

[11] D. D. Liang, S. X. Ng. Soon, and L. Hanzo, "Soft-decision star-QAM aided BICM-ID," *IEEE Signal Processing Letters*, vol. 18, no. 3, pp. 169-172, Mar. 2011.

[12] C. Xu, D. Liang, S. X. Ng, and L. Hanzo, "Reduced-complexity noncoherent soft-decision-aided DAPSK dispensing with channel estimation," *IEEE Transactions on Vehicular Technology.*, vol. 62, no. 6, pp. 2633-2643, July 2013.

[13] *Evolved Universal Terrestrial Radio Access (E-UTRA); Physical Channels and Modulation*, 3GPP Standard TS 36.211, V8.2.0 (2008-03), Release 8.

[14] *Evolved Universal Terrestrial Radio Access (E-UTRA); Further advancements for E-UTRA physical layer aspects*, 3GPP TR 36.814, V9.0.0 (2012-03), Release 9.

[15] *Evolved Universal Terrestrial Radio Access (E-UTRA); Physical layer procedures*, 3GPP TS 36.213 V8.8.0, Release 8, (2009-10).

[16] R. Jain, "Channel Models: A tutorial," *WiMAX forum AATG*, Ferbruray 2007.